

Seeking Necessary and Sufficient Information from Multimodal Medical Data

Boyu Chen^{1*}, Weiye Bao^{2*}, Junjie Liu², Michael Shen³, Bo Peng¹, Paul Taylor¹, Zhu Li³[✉], and Mengyue Yang⁴[✉]

¹ University College London, London, UK

² Imperial College London, London, UK

³ Mingdu Tech, China

⁴ University of Bristol, Bristol, UK

Abstract. Learning multimodal representations from medical images and other data sources can provide richer information for decision-making. While various multimodal models have been developed for this, they overlook learning features that are both necessary (must be present for the outcome to occur) and sufficient (enough to determine the outcome). We argue learning such features is crucial as they can improve model performance by capturing essential predictive information, and enhance model robustness to missing modalities as each modality can provide adequate predictive signals. Such features can be learned by leveraging the Probability of Necessity and Sufficiency (PNS) as a learning objective, an approach that has proven effective in unimodal settings. However, extending PNS to multimodal scenarios remains underexplored and is non-trivial as key conditions of PNS estimation are violated. We address this by decomposing multimodal representations into modality-invariant and modality-specific components, then deriving tractable PNS objectives for each. Experiments on synthetic and real-world medical datasets demonstrate our method’s effectiveness. Code will be available on GitHub.

Keywords: Representation Learning · Multi-modality · Probability of Necessity and Sufficiency.

1 Introduction

Multimodal representation learning has become essential in medical imaging, as integrating multiple data sources provides richer information for prediction. Various multimodal models have been developed for this task, such as multimodal fusion [16, 27, 5, 12, 18], contrastive learning [14, 26, 22, 25, 9], and disentanglement [3, 20, 11, 7]. However, they overlook the importance of learning the features that are both necessary and sufficient for the outcome.

Necessity means a feature must be present for the outcome to occur, but its presence alone does not confirm the outcome (e.g., pulmonary infiltrates on chest

* These authors contributed equally.

✉ Corresponding author.

CT are typical in pneumonia, but infiltrates alone are not diagnostic). Sufficiency means a feature can confirm the outcome when present, but it may be absent even if the outcome occurs (e.g., a visible pneumothorax line on chest X-ray confirms pneumothorax, but early pneumothorax may lack this line). Ideally, predictive features are both necessary and sufficient (e.g., a fracture line on X-ray indicates a fracture, and fractures present with such lines).

Learning such features provides advantages for multimodal medical data. First, it improves predictive performance: necessity ensures critical information is captured, while sufficiency guarantees the captured information is predictive [23, 1, 2]. Second, it can handle missing modalities, which is a pervasive challenge in clinical practice [16, 27, 5, 6, 11]. When each modality learns to capture necessary and sufficient features, any available subset of modalities retains adequate predictive signal, enabling robust inference with incomplete data.

Recent work has applied the Probability of Necessity and Sufficiency (PNS) to learn such features in unimodal data [23, 21, 4, 1, 2]. However, extending PNS to multimodal settings remains underexplored and is non-trivial as key conditions of PNS estimation are violated (details in section 2). We address this by decomposing multimodal representations into modality-invariant and modality-specific components, then deriving tractable PNS objectives for each. Experiments on synthetic and real-world medical datasets show the effectiveness of our method.

2 Preliminaries

This section covers PNS computation, challenges in multimodal extension, and representation decoupling—foundations for our method in section 3.

PNS is the probability of a feature set being both necessary and sufficient for an outcome. Let $Z \subset \mathbb{R}^{d_z}$ be the features of outcome $Y \subset \mathbb{R}^{d_y}$, where z and \bar{z} are two distinct values of Z . The PNS of Z with respect to Y for z and \bar{z} is defined as: $\text{PNS}(z, \bar{z}) := P(Y_{\text{do}(Z=z)} = y | Z = \bar{z}, Y \neq y) \cdot P(Z = \bar{z}, Y \neq y) + P(Y_{\text{do}(Z=\bar{z})} \neq y | Z = z, Y = y) \cdot P(Z = z, Y = y)$ [19, 23].

The do-operator $\text{do}(Z = z)$ denotes an intervention setting Z to z , which cannot be directly computed from observational data. However, under two conditions, PNS can be estimated using observational data:

Definition 1 (Exogeneity [19]). Z is exogenous to Y if Z has a direct effect on Y without confounding factors, i.e., $P(Y_{\text{do}(Z=z)} = y) = P(Y = y | Z = z)$.

Definition 2 (Monotonicity [19]). Y is monotonic w.r.t. Z when $(Y_{\text{do}(Z=z)} \neq y) \wedge (Y_{\text{do}(Z=\bar{z})} = y)$ or $(Y_{\text{do}(Z=z)} = y) \wedge (Y_{\text{do}(Z=\bar{z})} \neq y)$ is false, which can be presented as: $P(Y_{\text{do}(Z=z)} = y)P(Y_{\text{do}(Z=\bar{z})} \neq y) = 0$ or $P(Y_{\text{do}(Z=z)} \neq y)P(Y_{\text{do}(Z=\bar{z})} = y) = 0$.

Lemma 1 ([19]). Under monotonicity and exogeneity:

$$\text{PNS}(z, \bar{z}) = P(Y = y | Z = z) - P(Y = y | Z = \bar{z})$$

Recent studies have applied PNS to guide representation learning in unimodal data [23, 21, 4, 1, 2], but extending it to multimodal scenarios faces challenges in satisfying these two conditions. Exogeneity is violated since interactions across modalities can introduce hidden confounding effects without strong assumptions [23, 21, 17, 15]. Without exogeneity, the interventional probabilities in definition 2 cannot be converted to conditional probabilities, making it intractable to establish monotonicity from observational data.

To address these challenges, our work builds upon the assumption that multimodal data can be decoupled into two types of latent variables: one shared across modalities and the other conditioned on the modality type [3, 20, 11, 13]. As illustrated in fig. 1(a), the data generation process involves two latent factors. Let (X^1, \dots, X^N, Y) be a multimodal sample with N modalities, abbreviated as (X, Y) , where $X^M \subset \mathbb{R}^{d_M}$ denotes the input from modality M and $Y \subset \mathbb{R}^{d_y}$ denotes the outcome. A modality sample (X^M, Y) is generated from: a modality-invariant latent variable $Z_I \subset \mathbb{R}^{d_{z_I}}$ capturing shared information across modalities, and modality-specific latent variables $Z_S \subset \mathbb{R}^{d_{z_S}}$ conditioned on modality type M , encoding characteristics unique to each modality [3, 20, 11, 13].

A decoupling (or disentanglement) $\mathcal{D}(\cdot)$ model aims to capture information from these latent factors by extracting two types of representations from X^M : modality-invariant representations $\mathcal{R}_I^M \subset \mathbb{R}^{d_{z_I}}$ approximating Z_I , and modality-specific representations $\mathcal{R}_S^M \subset \mathbb{R}^{d_{z_S}}$ approximating Z_S conditioned on modality type M . A typical architecture of $\mathcal{D}(\cdot)$ (shown in fig. 1(b)) which consists of a feature extractor $\Phi(\cdot)$ that decouples the representations $[\mathcal{R}_I^M, \mathcal{R}_S^M] := \phi(X^M)$, and three types of predictors: (1) modality-specific predictors $F_M(\cdot)$ predicting Y from \mathcal{R}_S^M ; (2) an invariant predictor $F_I(\cdot)$ predicting Y from \mathcal{R}_I^M ; (3) a joint predictor $F_P(\cdot)$ predicting Y from all representations. We denote the overall model prediction as $\hat{Y} = \mathcal{D}(X)$. The training objective is:

$$\mathcal{L}^D := \mathcal{L}_{pred} + \mathcal{L}_{dec} + \sum_{M=1}^N (\mathcal{L}_I^M + \mathcal{L}_S^M) \quad (1)$$

where $\mathcal{L}_I^M := \mathcal{L}_I^M(F_I(\mathcal{R}_I^M), Y)$ and $\mathcal{L}_S^M := \mathcal{L}_S^M(F_M(\mathcal{R}_S^M), Y)$ measure the prediction accuracy of \mathcal{R}_I^M and \mathcal{R}_S^M , respectively, while $\mathcal{L}_{pred} := \mathcal{L}_{pred}(\mathcal{D}(X), Y)$ is the prediction loss, and \mathcal{L}_{dec} includes decoupling and other constraints. The specific architectures of feature extractors, predictors, and loss functions vary across prior multimodal decoupling work.

3 Method

Following section 2, we decompose representations into invariant and specific components, enabling separate PNS analysis for each.

3.1 Learning Complement Representations

Computing PNS via lemma 1 requires feature pairs (z, \bar{z}) where z predicts correctly while \bar{z} does not. We achieve this by generating complement representations $\bar{\mathcal{R}}_I^M$ and $\bar{\mathcal{R}}_S^M$ that predict incorrectly, in contrast to \mathcal{R}_I^M and \mathcal{R}_S^M . Specifically, as shown in fig. 1(c), we use a complement feature extractor $\phi(\cdot)$ that

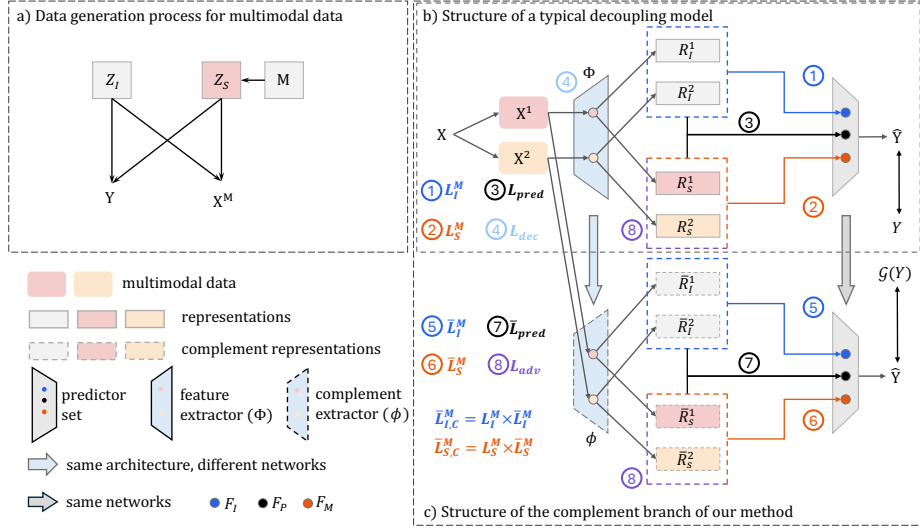


Fig. 1. Overview of the proposed MPNS framework. The figure shows the multimodal data generation process, a baseline decoupling model, and our proposed complement branch with PNS-based optimization.

mirrors the architecture of $\Phi(\cdot)$ but extracts $[\bar{\mathcal{R}}_I^M, \bar{\mathcal{R}}_S^M] := \phi(X^M)$. To train $\phi(\cdot)$ for incorrect predictions, we define a label generator $\mathcal{G}(\cdot)$ that randomly samples labels different from Y : $\bar{Y} = \mathcal{G}(Y)$. The complement extractor is optimized via:

$$\bar{\mathcal{L}}_{pred} := \mathcal{L}_{pred}(\mathcal{D}_\phi(X), \mathcal{G}(Y)) \quad (2)$$

where $\mathcal{D}_\phi(\cdot)$ denotes the decoupling model using $\phi(\cdot)$.

3.2 PNS for Modality-Invariant Representation

As illustrated in fig. 1(a), analyzing Z_I alone eliminates cross-modal confounding, making it exogenous to Y since no other variable acts as a confounder between them. Under monotonicity, lemma 1 enables tractable PNS estimation from observational data. This reduces to the unimodal setting, and therefore we adopt the PNS-based objective from [23] for the invariant component of modality M , which can capture necessary and sufficient information:

$$\mathcal{L}_{M,I}^{pns} := \mathcal{L}_I^M + \bar{\mathcal{L}}_I^M + \mathcal{L}_{I,C}^M \quad (3)$$

where \mathcal{L}_I^M (from eq. (1)) maximizes $P(Y = y | Z_I = z)$ by training $F_I(\mathcal{R}_I^M)$ to predict Y accurately, and $\bar{\mathcal{L}}_I^M := \mathcal{L}_I^M(F_I(\bar{\mathcal{R}}_I^M), \mathcal{G}(Y))$ minimizes $P(Y = y | Z_I = \bar{z})$ by enforcing $F_I(\bar{\mathcal{R}}_I^M)$ predicts away from Y .

The constraint term $\mathcal{L}_{I,C}^M := \mathcal{L}_I^M \times \bar{\mathcal{L}}_I^M$ enforces modality monotonicity by minimizing $P(Y \neq y | Z_I = z) \cdot P(Y = y | Z_I = \bar{z}) = P(Y_{do(Z_I=z)} \neq y) \cdot P(Y_{do(Z_I=\bar{z})} = y)$ from definition 2.

3.3 PNS for Modality-Specific Representation

Unlike the modality-invariant component, the modality-specific component is conditioned on M , violating exogeneity (fig. 1(a)). As such, we propose to approximate exogeneity by enforcing $\mathcal{R}_S^M \perp M$ on the learned representations.

We use adversarial training to achieve this. Specifically, a modality discriminator is trained to classify M from \mathcal{R}_S^M , while feature extractors $\Phi(\cdot)$ and $\phi(\cdot)$ simultaneously learn to produce representations that fool the discriminator via gradient reversal layer (GRL) [8], and maintaining predictive power for outcomes. We define the adversarial loss as \mathcal{L}_{adv} .

Note that $\mathcal{R}_S^M \perp M$ removes dependence on modality identity (preventing the model from learning "this is modality M ") but not on modality-specific content. Unlike \mathcal{R}_I , which captures shared information across modalities, \mathcal{R}_S^M still encodes information unique to that modality via $\mathcal{D}(\cdot)$. The independence constraint encourages \mathcal{R}_S^M to learn these unique features based on their diagnostic value rather than on artifacts of modality type M .

When we break the dependency between \mathcal{R}_S^M and M , lemma 1 can be applied analogously to the modality-invariant case. The PNS objective for M is:

$$\mathcal{L}_{M,S}^{pns} := \mathcal{L}_S^M + \bar{\mathcal{L}}_S^M + \mathcal{L}_{S,C}^M \quad (4)$$

where \mathcal{L}_S^M (from eq. (1)) encourages high $P(Y = y \mid Z_S = z)$ by training $F_M(\mathcal{R}_S^M)$ to predict Y accurately, $\bar{\mathcal{L}}_S^M := \mathcal{L}_S^M(F_M(\bar{\mathcal{R}}_S^M), \mathcal{G}(Y))$ minimizes $P(Y = y \mid Z_S = \bar{z})$, and $\mathcal{L}_{S,C}^M := \mathcal{L}_S^M \times \bar{\mathcal{L}}_S^M$ enforces monotonicity, mirroring eq. (3). Some decoupling models may not include modality-specific $F_M(\cdot)$. In such cases, $F_M(\cdot)$ can be implemented by adapting the architecture of $F_I(\cdot)$ or $F_P(\cdot)$.

3.4 Multimodal Representation Learning via PNS

Our framework are shown in fig. 1(c) and the final objective is:

$$\mathcal{L}^{pns} := \mathcal{L}^D + \bar{\mathcal{L}}_{pred} + \mathcal{L}_{adv} + \sum_{M=1}^N (\bar{\mathcal{L}}_I^M + \mathcal{L}_{I,C}^M + \bar{\mathcal{L}}_S^M + \mathcal{L}_{S,C}^M) \quad (5)$$

We name our approach MPNS (Multimodal Representation Learning via PNS). The implementation is straightforward (fig. 1(c)): add a complement extractor $\phi(\cdot)$ and the adversarial training to the base model $\mathcal{D}(\cdot)$, and optimize \mathcal{L}^{pns} jointly. At inference, only $\mathcal{D}(\cdot)$ is retained. This makes MPNS a plug-and-play framework that introduces no additional inference cost.

4 Experiments and Results

We constructed synthetic datasets to verify the ability of MPNS to capture necessary and sufficient information for representations. Then, we used real-world multimodal MRI datasets to show the improvement and robustness brought by MPNS. All experiments were conducted on $4 \times$ NVIDIA GH200 GPUs.

Table 1. Distance Correlation based on s for modality 1 and 2

Mode	Modality 1				Modality 2				
	NS	SF	NC	SC	NS	SF	NC	SC	
$s = 0.0$	w/o PNS	0.626	0.667	0.658	0.291	0.519	0.607	0.646	0.312
	w/o $\mathcal{L}_{M,I}^{pns}$	0.645	0.681	0.665	0.294	0.536	0.597	0.633	0.323
	w/o $\mathcal{L}_{M,S}^{pns}$	0.663	0.673	0.644	0.305	0.627	0.577	0.636	0.349
	MPNS	0.682	0.658	0.578	0.298	0.649	0.553	0.629	0.364
$s = 0.3$	w/o PNS	0.613	0.682	0.645	0.322	0.520	0.618	0.614	0.347
	w/o $\mathcal{L}_{M,I}^{pns}$	0.631	0.683	0.643	0.316	0.541	0.607	0.608	0.343
	w/o $\mathcal{L}_{M,S}^{pns}$	0.644	0.691	0.591	0.322	0.621	0.591	0.617	0.377
	MPNS	0.661	0.657	0.572	0.323	0.640	0.564	0.617	0.394
$s = 0.7$	w/o PNS	0.619	0.683	0.664	0.352	0.503	0.614	0.636	0.371
	w/o $\mathcal{L}_{M,I}^{pns}$	0.635	0.696	0.678	0.361	0.521	0.602	0.642	0.369
	w/o $\mathcal{L}_{M,S}^{pns}$	0.666	0.683	0.602	0.364	0.633	0.574	0.630	0.412
	MPNS	0.678	0.652	0.585	0.361	0.647	0.548	0.599	0.448

4.1 Synthetic Multimodal Dataset Experiments

To verify MPNS’s ability to learn high-PNS representations, we followed the protocol from [23]: 1) generate a variable, called necessary and sufficient variable NS , that directly determines the outcome; 2) generate other variables with different properties; 3) mix them as latent variables; 4) transform them by non-linear functions to create observed data; 5) train models on the observed data to learn representations; 6) measure how well representations capture the original latent variables via Distance Correlation (DC) [10], where higher DC with NS indicates better high-PNS learning. We extend this to multimodal settings:

We first generated the latent variables and outcome using the same method as [23]: **Necessary and Sufficient variable** NS is a deterministic variable sampled from a Bernoulli distribution $B(0.5)$ and determines the outcome $Y = NS \oplus B(0.15)$, where \oplus is the XOR operation. **Sufficient but Unnecessary variable** $SF \sim B(0.1)$ if $NS=0$; $SF=1$ if $NS=1$. **Necessary but Insufficient variable** $NC = I(NS = 1) \cdot B(0.9)$, where $I(\cdot)$ is an indicator function. **Spurious correlation variable** SC is generated to spuriously correlate with NS , defined as $s \cdot NS + (1 - s)\mathcal{N}(0, 1)$, where $s \in [0, 1)$ is spurious correlation level and $\mathcal{N}(0, 1)$ is a standard Gaussian distribution.

Then, We generated observed data with two modalities from latent variables. We construct a vector $h = [NS \cdot \mathbf{1}_d, SF \cdot \mathbf{1}_d, NC \cdot \mathbf{1}_d, SC \cdot \mathbf{1}_d] + \mathcal{N}(0, 0.3)$, where $\mathbf{1}_d$ is a d -dimensional all-ones vector and Y is determined by NS . For each variable type, we use the first, middle, and last $d/3$ dimensions of each type as modality-invariant (z_1) and modality-specific (z_2 and z_3) components. The non-linear function is $\kappa(z, \beta) = \beta \cdot \tanh(z)$, and $[\cdot, \cdot]$ denotes concatenation of column vectors. The two modalities are then generated as $X^1 = \kappa([z_1, \kappa(z_2, \beta_1)], \beta_2)$ and $X^2 = \kappa([z_1, \kappa(z_3, \beta_3)], \beta_4)$. We set $(\beta_1, \beta_2, \beta_3, \beta_4) = (2.0, 1.8, 1.5, 1.2)$ and $d = 15$.

Next, we trained models on the observed data. We used DMD [13], a state-of-the-art (SOTA) multimodal decoupling model, as the base model of MPNS. We also conducted ablation studies: 1) **w/o PNS**. original DMD is optimized only with \mathcal{L}^D in eq. (1); 2) **w/o $\mathcal{L}_{M,I}^{pns}$** . only \mathcal{L}_I^M is optimized in eq. (3); 3) **w/o $\mathcal{L}_{M,S}^{pns}$** .

Table 2. Dice coefficients on BraTS2020 with missing modalities. Notes: ●/○: available/missing modality. **Bold/underlined**: **best/second-best** result. †: MPNS outperforms its base decoupling model.

Subregions	F	T1	T1c	T2	RobustSeg	RFNet	mmFormer	M ³ AE	ShaSpec	ShaSpec (MPNS)	DC-Seg	DC-Seg (MPNS)	
Whole	○	○	○	●	82.20	<u>86.05</u>	85.51	86.10	83.98	83.86	85.16	85.09	
	○	○	●	○	71.39	76.77	78.04	<u>78.90</u>	76.18	76.91 [†]	78.57	79.45 [†]	
	○	●	○	○	71.41	77.16	76.24	79.00	74.27	74.65 [†]	<u>77.33</u>	76.96	
	●	○	○	○	82.87	87.32	86.54	88.00	89.25	89.25	88.86	<u>89.01</u> [†]	
	○	○	●	●	85.97	87.74	87.52	87.10	86.57	86.21	<u>87.94</u>	88.07 [†]	
	○	●	●	○	76.84	81.12	80.70	80.10	78.92	78.90	<u>81.99</u>	82.00 [†]	
	●	●	○	○	88.10	89.73	88.76	89.60	90.31	90.31	90.03	<u>90.06</u> [†]	
	○	●	○	●	85.53	87.73	86.94	87.30	85.42	85.77 [†]	87.13	<u>87.39</u> [†]	
	●	○	○	●	88.09	89.87	89.49	90.10	<u>90.43</u>	90.41	90.06	91.07 [†]	
	●	○	●	○	87.33	89.89	89.31	89.50	90.34	90.43 [†]	90.31	<u>90.36</u> [†]	
	●	●	●	○	88.87	90.69	89.79	89.60	90.60	90.54	<u>90.83</u>	90.90 [†]	
	●	●	○	○	89.24	90.60	89.83	90.20	<u>90.65</u>	90.61	90.59	90.74 [†]	
	○	○	●	●	88.68	90.68	90.49	90.50	90.89	<u>90.90</u> [†]	90.76	91.35 [†]	
	○	●	●	●	86.63	88.25	87.64	87.40	86.94	86.49	<u>88.24</u>	88.23	
	●	●	●	●	89.47	91.11	90.54	90.40	<u>91.04</u>	90.91	90.93	90.94 [†]	
		Average				84.17	86.98	86.49	86.90	86.39	86.41 [†]	<u>87.25</u>	87.44 [†]
	Core	○	○	○	●	61.88	<u>71.02</u>	63.36	71.80	65.57	65.58 [†]	68.09	69.58 [†]
○		○	●	○	76.68	81.51	81.51	83.60	80.60	80.87 [†]	<u>83.31</u>	83.30	
○		●	○	○	54.30	66.02	63.23	69.40	63.72	65.20 [†]	65.85	<u>66.14</u> [†]	
●		○	○	○	60.72	69.19	64.60	68.70	69.15	69.79 [†]	<u>70.26</u>	71.40 [†]	
○		○	●	●	82.44	83.45	82.69	85.60	81.94	81.66	83.82	<u>84.38</u> [†]	
○		●	●	○	80.28	83.40	82.81	83.80	82.01	81.45	<u>84.35</u>	84.40 [†]	
●		●	○	○	68.18	73.07	71.76	72.80	72.93	<u>73.37</u> [†]	73.81	72.98	
○		○	○	●	66.46	73.13	67.76	<u>72.90</u>	68.51	69.36 [†]	70.40	71.70 [†]	
●		○	○	●	68.20	74.14	70.34	<u>74.30</u>	71.58	71.97 [†]	73.43	75.33 [†]	
●		○	●	○	81.85	<u>84.65</u>	83.79	85.50	82.39	82.37	<u>84.65</u>	83.91	
●		●	○	○	82.76	<u>85.07</u>	84.44	85.60	83.08	82.83	84.88	83.84	
●		●	○	●	70.46	<u>75.19</u>	72.42	74.40	72.54	73.13 [†]	73.75	75.47 [†]	
○		○	●	○	81.89	<u>84.97</u>	83.94	85.80	82.44	82.00	84.25	84.63 [†]	
○		●	●	●	82.85	<u>83.47</u>	83.66	85.80	82.70	82.07	<u>84.70</u>	84.37	
●		●	●	●	82.87	<u>85.21</u>	84.61	86.20	82.98	82.38	84.27	84.49 [†]	
		Average				73.45	78.23	76.06	79.10	76.14	76.27 [†]	77.99	<u>78.39</u> [†]
Enhancing		○	○	○	●	36.46	46.29	49.09	47.10	42.31	41.22	47.14	<u>47.35</u> [†]
	○	○	●	○	67.91	74.85	78.30	73.60	72.83	72.87 [†]	76.68	<u>76.74</u> [†]	
	○	●	○	○	28.99	37.30	37.62	40.40	38.61	39.52 [†]	<u>40.73</u>	42.47 [†]	
	○	○	○	○	34.68	38.15	36.68	40.20	44.09	43.54	44.98	<u>44.29</u>	
	○	○	●	●	71.42	75.93	77.20	76.00	73.95	73.56	76.09	<u>76.68</u> [†]	
	○	○	●	○	70.11	<u>78.01</u>	81.71	75.30	73.40	73.55 [†]	76.96	77.25 [†]	
	○	●	○	○	39.67	40.98	42.98	43.70	46.65	47.54 [†]	<u>47.97</u>	49.57 [†]	
	○	●	○	●	39.92	45.65	<u>49.12</u>	48.70	45.28	45.04	48.76	51.27 [†]	
	●	○	○	●	42.19	49.32	49.06	47.10	46.25	46.72 [†]	52.01	<u>51.98</u>	
	○	○	●	○	70.78	76.67	79.44	75.90	74.12	74.25 [†]	76.66	<u>77.01</u> [†]	
	●	●	●	○	71.77	76.81	80.65	76.30	74.17	74.59 [†]	<u>77.74</u>	77.50	
	●	●	○	●	43.90	49.92	50.08	48.20	47.62	48.69 [†]	<u>52.84</u>	55.43 [†]	
	○	○	●	○	71.17	77.12	78.73	<u>77.40</u>	73.95	73.93	76.57	77.25 [†]	
	○	○	●	●	71.87	<u>76.99</u>	77.34	78.00	74.13	73.96	76.16	76.28 [†]	
	●	●	●	●	71.52	<u>78.00</u>	79.92	77.50	73.96	74.37 [†]	76.83	76.43	
		Average				55.49	61.47	63.19	61.70	60.09	60.22 [†]	<u>63.21</u>	63.83 [†]
	Average					71.04	75.56	75.25	75.90	74.21	74.30 [†]	<u>76.15</u>	76.55 [†]

only \mathcal{L}_S^M is optimized in eq. (4); and 4) **MPNS**, the full model trained with complete \mathcal{L}^{pns} . We varied s as 0.0, 0.3 and 0.7 to show the different spurious correlation levels. We generated 15,000 training and 5,000 evaluation samples for each s . Results are shown on table 1.

4.2 Real-world Multimodal Medical Dataset Experiments

We evaluated MPNS on BraTS2020 [24], a widely used multimodal MRI dataset for brain tumor segmentation. It contains four MRI modalities (FLAIR, T1c, T1, T2) with segmentation masks for three tumor sub-regions (whole tumor, tumor core, and enhancing tumor), and has 369 cases split into 219/50/100 for training/validation/testing. We compared against SOTA and open-sourced multimodal medical segmentation methods: RobustSeg [3], RFNet [5], mmFormer [27], M³AE [16], ShaSpec [20], and DC-Seg [11]. Among these, ShaSpec and DC-Seg are decoupling models, and serve as our base architectures of MPNS. Results are shown on Table 2.

4.3 Results and Discussion

Table 1 shows DC between representations and latent variables, where higher DC with NS indicates better representation. DMD with MPNS consistently outperforms all variants. As s increases, DC with SC also rises for all models but MPNS still has a strong correlation with NS . Removing $\mathcal{L}_{M,I}^{pns}$ causes more performance drop than removing $\mathcal{L}_{M,S}^{pns}$, suggesting that our method can capture more necessary and sufficient information from the modality-invariant component in data. The reason could be that invariant components naturally satisfy exogeneity while specific components need approximation. These results show that our MPNS can capture more necessary and sufficient information from data.

Table 2 compares our method against baselines under missing modality scenarios. MPNS improves the performance of both base decoupling models (ShaSpec and DC-Seg), outperforming the baselines in most cases. This shows that learning high-PNS representations can enhance both the performance and robustness of multimodal models.

Our work introduces PNS to multimodal representation learning and could open promising avenues for future research, despite certain limitations. First, our method’s effectiveness depends on the base decoupling model’s disentanglement quality. When decoupling is suboptimal (e.g., for the core region in table 2), our performance gains are limited. As multimodal disentanglement remains an active research area, advances in decoupling models could further enhance our approach. Second, we approximate exogeneity for modality-specific representations via adversarial training, but alternative strategies merit exploration. Third, our method captures necessary and sufficient features within individual modalities, while such features may also emerge from cross-modal combinations. Fourth, our current formulation focuses on discrete outcomes, while extending to continuous outcomes requires further investigation. Extending PNS to capture these joint patterns represents a promising direction. By introducing PNS to multimodal learning, our work provides insights for future research in multimodal representation learning and related domains.

5 Conclusion

We introduce PNS to guide multimodal medical representation learning and propose a method that promotes high-PNS representations. Experiments on synthetic and real-world datasets show that our method can learn high-PNS representations and improve the performance and robustness of multimodal models.

References

1. Cai, H., Wang, Y., Jordan, M., Song, R.: On learning necessary and sufficient causal graphs. *NeurIPS'23* **36**, 42148–42160 (2023)
2. Chen, B., Solebo, A.L., Bao, W., Taylor, P.: Medical image quality assessment based on probability of necessity and sufficiency. In: *ISBI'25*. pp. 1–4. IEEE (2025)
3. Chen, C., Dou, Q., Jin, Y., Chen, H., Qin, J., Heng, P.A.: Robust multimodal brain tumor segmentation via feature disentanglement and gated fusion. In: *MICCAI'19*. pp. 447–456. Springer (2019)
4. Chen, X., Cai, R., Zheng, K., Jiang, Z., Huang, Z., Hao, Z., Li, Z.: Unifying invariance and spuriousity for graph out-of-distribution via probability of necessity and sufficiency. *arXiv preprint arXiv:2402.09165* (2024)
5. Ding, Y., Yu, X., Yang, Y.: Rfnet: Region-aware fusion network for incomplete multi-modal brain tumor segmentation. In: *ICCV'21*. pp. 3975–3984 (2021)
6. D'Souza, N.S., Wang, H., Giovannini, A., Foncubierto-Rodriguez, A., Beck, K.L., Boyko, O., Syeda-Mahmood, T.: Fusing modalities by multiplexed graph neural networks for outcome prediction in tuberculosis. In: *MICCAI'22*. pp. 287–297. Springer (2022)
7. Eijpe, A., Lakbir, S., Erdal Cesur, M., Oliveira, S.P., Abeln, S., Silva, W.: Disentangled and interpretable multimodal attention fusion for cancer survival prediction. In: *MICCAI'25*. pp. 117–127. Springer (2025)
8. Ganin, Y., Ustinova, E., Ajakan, H., Germain, P., Larochelle, H., Laviolette, F., March, M., Lempitsky, V.: Domain-adversarial training of neural networks. *Journal of machine learning research* **17**(59), 1–35 (2016)
9. Gu, Y., Saito, K., Ma, J.: Learning contrastive multimodal fusion with improved modality dropout for disease detection and prediction. In: *MICCAI'25*. pp. 280–290. Springer (2025)
10. Jones, T., Forrest, S., et al.: Fitness distance correlation as a measure of problem difficulty for genetic algorithms. In: *ICGA*. vol. 95, pp. 184–192 (1995)
11. Li, H., Li, Z., Mao, Y., Ding, Z., Huang, Z.: Dc-seg: Disentangled contrastive learning for brain tumor segmentation with missing modalities. In: *MICCAI'25*. pp. 138–148. Springer (2025)
12. Li, R., Li, C., Lin, X., Xu, J., Li, F., Lu, Y.: Multimodal fusion network with distribution-based tumor-marker imputation for multi-origin metastatic cervical lymphadenopathy classification. In: *MICCAI'25*. pp. 450–459. Springer (2025)
13. Li, Y., Wang, Y., Cui, Z.: Decoupled multimodal distilling for emotion recognition. In: *CVPR'23*. pp. 6631–6640 (2023)
14. Lin, W., Zhao, Z., Zhang, X., Wu, C., Zhang, Y., Wang, Y., Xie, W.: Pmc-clip: Contrastive language-image pre-training using biomedical documents. In: *MICCAI'23*. pp. 525–536. Springer (2023)
15. Liu, C., Sun, X., Wang, J., Tang, H., Li, T., Qin, T., Chen, W., Liu, T.Y.: Learning causal semantic representation for out-of-distribution prediction. *NeurIPS'21* **34**, 6155–6170 (2021)
16. Liu, H., Wei, D., Lu, D., Sun, J., Wang, L., Zheng, Y.: M3ae: multimodal representation learning for brain tumor segmentation with missing modalities. In: *AAAI'23*. vol. 37, pp. 1657–1665 (2023)
17. Locatello, F., Bauer, S., Lucic, M., Raetsch, G., Gelly, S., Schölkopf, B., Bachem, O.: Challenging common assumptions in the unsupervised learning of disentangled representations. In: *ICML'19*. pp. 4114–4124. PMLR (2019)

18. Ma, D., Cao, J., Cheng, H., Zhou, D., Liu, J., Zhang, X., Wu, K., Gu, C., Guan, X.: Longitudinal mri-clinical multimodal fusion for pcr prediction in breast cancer. In: MICCAI'25. pp. 323–332. Springer (2025)
19. Pearl, J.: Causality. Cambridge university press (2009)
20. Wang, H., Chen, Y., Ma, C., Avery, J., Hull, L., Carneiro, G.: Multi-modal learning with missing modality via shared-specific feature modelling. In: CVPR'23. pp. 15878–15887 (2023)
21. Wang, Y., Jordan, M.I.: Desiderata for representation learning: A causal perspective. *Journal of Machine Learning Research* **25**(275), 1–65 (2024)
22. Wang, Z., Wu, Z., Agarwal, D., Sun, J.: Medclip: Contrastive learning from unpaired medical images and text. In: EMNLP'22. pp. 3876–3887 (2022)
23. Yang, M., Fang, Z., Zhang, Y., Du, Y., Liu, F., Ton, J.F., Wang, J., Wang, J.: Invariant learning via probability of sufficient and necessary causes. *NeurIPS'23* **36**, 79832–79857 (2023)
24. Zadeh, A.B., Liang, P.P., Poria, S., Cambria, E., Morency, L.P.: Multimodal language analysis in the wild: Cmu-mosei dataset and interpretable dynamic fusion graph. In: ACL'18. pp. 2236–2246 (2018)
25. Zhang, D., Xiao, W., Jiang, C., Qiu, Y., Feng, Z., Wang, H., Zheng, Y., Zhu, W.: A multimodal contrastive learning for detecting aortic dissection on 3d non-contrast ct with anatomy simplification. In: MICCAI'25. pp. 3–12. Springer (2025)
26. Zhang, S., Zhang, J., Tian, B., Lukasiewicz, T., Xu, Z.: Multi-modal contrastive mutual learning and pseudo-label re-learning for semi-supervised medical image segmentation. *Medical Image Analysis* **83**, 102656 (2023)
27. Zhang, Y., He, N., Yang, J., Li, Y., Wei, D., Huang, Y., Zhang, Y., He, Z., Zheng, Y.: mmformer: Multimodal medical transformer for incomplete multimodal learning of brain tumor segmentation. In: MICCAI'22. pp. 107–117. Springer (2022)